Connection between Simple Models and Quantum Chemical Models for Electron-Transfer Tunneling Matrix Element Calculations: A Dyson's Equations-Based Approach

Ilya A. Balabin[†] **and José Nelson Onuchic***

Department of Physics, University of California at San Diego, 9500 Gilman Drive, La Jolla, California 92093-0319

Received: December 1, 1995; In Final Form: May 15, 1996[⊗]

Pathwaylike models for electron transfer (ET) are based on simple Hamiltonians that are tuned to provide the proper wave function distance decay and sign alternation of the wave function with every bond. This alternation plays a vital role on interference effects among different tubes. To verify the validity of these models and to obtain "quantitative effective" parameters (at extended Hückel level) to use in pathwaylike Hamiltonians, a series of calculations (exact and approximate) has been performed for several ideal chainlike bridges. Particular emphasis is given to the dependence on the tunneling energy, length of interaction among orbitals, side groups, boundary effects, and nonorthogonality of the orbital basis. We also show how the ET rate along a single physical pathway is determined by competition among several ET decay modes.

Introduction

Electron transfer (ET) plays a key role in many chemical, biological, and physical processes. In biology, these reactions are exceptionally important in bioenergetic processes such as photosynthesis and oxidative phosphorylation.[1] In typical biological ET systems, localized donor (D) and acceptor (A) states are embedded in a protein matrix far apart from each other so that the direct electronic coupling between them is extremely small. In such systems, the tunneling matrix element is determined by intermediate ("bridge") electronic states provided by the protein or cofactors between the D and A. This kind of ET mechanism has been first proposed by McConnell.[2] The rates of bridge-mediated, or superexchange, ET reactions are known to be in some cases remarkably sensitive to the structure of the bridge. Understanding how molecular and electronic structure controls the electronic coupling is vital for both understanding biological ET reactions and designing new ET proteins.[3−13]

Most superexchange ET reactions are essentially nonadiabatic, so their rate is given by the Fermi "Golden Rule" expression

$$k_{\mathrm{ET}} = \frac{2\pi}{\hbar}|T_{\mathrm{DA}}|^2\mathrm{FC} \tag{1}$$

where T_{DA} is the effective DA electronic coupling provided by the bridge. FC is the Frank−Condon factor that incorporates the nuclear effects. In this work, we focus on the electronic tunneling matrix element, which, for an orthogonal basis, can be written as[5,14]

$$T_{\mathrm{DA}} = \sum_{i,j}^{\mathrm{bridge}} \beta_{\mathrm{D}i} G_{ij}(E_{\mathrm{t}}) \beta_{j\mathrm{A}} \tag{2}$$

where $\beta_{\mathrm{D}i}$ and $\beta_{j\mathrm{A}}$ are the electronic couplings of D and A with the bridge orbitals. The $G_{ij}(E_{\mathrm{t}})$'s are the electronic tunneling matrix elements of the bridge Green's function operator $\hat{G}(E_{\mathrm{t}}) = (E_{\mathrm{t}} - \hat{H})^{-1}$ that are dependent on the tunneling energy E_{t}. There is a need for effective methods for calculating this Green's function, one of the most difficult parts of the ET problem in general, especially for large biological molecules such as proteins.

Two approaches to calculate Green's functions seem mostly common. The first one is based on quantum chemical methods to compute a Hamiltonian (or Fock) matrix using a self-consistent energy minimization algorithm. Then, the Green's function is computed by matrix inversion techniques.[8,9,15,16] Depending on the required accuracy, different quantum chemical methods are chosen, from simple empirical ones, such as the extended Hückel method,[8,9,17,18] up to *ab initio* calculations,[6,19,20] which should, in principle, provide results as precise as necessary. In practice, however, *ab initio* calculations can be performed, even with supercomputers, only for relatively small molecular structures consisting of several atoms rather than for real proteins. Also, it is hard to extract from these calculations an understanding of the physical mechanisms controlling tunneling, which is one of the reasons why simple effective models are needed for studying ET. Most importantly, such simple models are vital for interpreting experiments and designing new ET systems.

On the spirit of simple effective models, pathwaylike approaches appear to be the most successful.[11−13,21−24] In these approaches, a simple Hamiltonian matrix, usually including only nearest-neighbor interactions among orbitals, is created, and the Green's function matrix elements are obtained by solving a linear system of Dyson's equations. In the case of periodic or nearly periodic molecular structures, e.g., protein backbone, the problem can be simplified, and the approach provides explicit analytical solution for the Green's function, making it possible to investigate how different features of molecular and electronic structure control ET rates. These approaches are especially fruitful for large biological molecules, and they have already been extremely successful in explaining qualitatively the effect of the the environment for ET in proteins. They have demonstrated that through-bond decay is much slower than through-space, that hydrogen bond paths are almost as good as covalent ones, and that aromatic groups are not as important as first believed. Several important questions, however, are still open and have to be addressed before a full quantitative ET model can be developed. For example, why does the electron wave function decay per site predicted by conventional path-

[†] E-mail: ibalabin@ucsd.edu, jonuchic@ucsd.edu.

[⊗] Abstract published in *Advance ACS Abstracts,* July 1, 1996.

S0022-3654(95)03568-4 CCC: $12.00

waylike methods[21,23] have a strong dependence on E_t (the experimental dependence, however, is softer, which is the reason why in the *Pathway* model[11,12] the E_t dependence was neglected). Also, understanding how the sign of the wave function changes with distance is vital for studying interference among tubes of pathways.[23,24]

For the reasons above, both, quantum chemical and simple effective Hamiltonian, methods should be considered as complementary rather than alternative. Our future goal is to integrate them into a new more powerful theoretical approach that provides a quantitative description of ET. As a first step, this paper addresses the question of how simple models should be extended to provide adequate results for biological molecules. Complex ET bridges may generate a collection of different tubes of pathways due to hydrogen bonds, through-space jumps, or nontrivial covalent bonding. Here we do not address any aspect of tube interference.[23,24] Instead, we focus on electron propagation along a series of ideal chainlike bridges, with the emphasis on two principal issues: (1) under what conditions simple effective Hamiltonian models provide valid predictions for such molecules and (2) how the ET rate along a chain depends on the orbital structures of the molecules. Dependence on the tunneling energy and the effects of the interactions between orbitals further than nearest neighbors, side groups, and, generally, nonorthogonal orbital basis are examined. The results for a series of analytical calculations, exact and approximate, are compared with the corresponding extended Hückel results. The structure of the ideal bridges and various approximations used in the calculations have been chosen in such a way as to probe each of these factors separately. The results are supposed to be used for obtaining new effective (E_t -dependent) interaction parameters for a new pathwaylike Hamiltonian.

Methods for Calculating Green's Functions

A. Numerical Approach: Quantum Chemical Calculations. The simplest possible method, extended Hückel, has been chosen for quantum chemical calculations.[25] Although it has been parametrized for computing electronic optical spectra rather than electron tunneling, it is still able to provide reasonable results with much smaller computational efforts than *ab initio* calculations.[26] The method is based on a single-particle tight-binding Hamiltonian explicitly treating the valence electrons. Standard parameters have been used with Slater-type nonorthogonal orbitals forming a minimal basis set of four valence orbitals per heavy atom and one per hydrogen atom.

The overlap matrix elements $S_{ij} = \langle i|j\rangle$ have been computed on an atomic orbital basis with the cutoff set at 10.0 Å. The diagonal Hamiltonian matrix elements are ionization potentials of atomic orbitals $H_{ii} = \langle i|\hat{H}|i\rangle = \alpha_i$; the off-diagonal elements are taken as $H_{ij} = (K/2)(\alpha_i + \alpha_j)S_{ij}$, where K is the Hückel constant. The overlap and Hamiltonian matrices are converted to hybrid (sp orbitals) or bond orbital basis sets by using standard transformations.[27] In order to study how various details of the electronic orbital structure affect the ET rate, a series of approximated calculations, in addition to exact ones (all orders of the interaction among the orbitals are included), have been performed: **(a)** nearest neighbor (NN) approximation, all couplings and overlaps are assumed to be zero, except between orbitals sharing the same atom (in hybrid basis—also between orbitals that form a bond); **(b)** next to nearest neighbor (NNN) approximation, all couplings and overlaps are assumed to be zero except between orbitals that have the same NN orbital; **(c)** complete neglect of overlap, overlap between different orbitals is assumed to be zero.

Because the orbital basis is generally nonorthogonal, the Green's function matrix **G** is computed not as a simple inversion of the $E_t\mathbf{I} - \mathbf{H}$ matrix but by projecting the operator definition of the Green's function $\hat{G} = (E_t - \hat{H})^{-1}$ on the desired basis. The resulting matrix equation is

$$\mathbf{G} = \mathbf{S}(E_t\mathbf{S} - \mathbf{H})^{-1}\mathbf{S} \tag{3}$$

B. Analytical Approach: Dyson's Equation-Based Method. Rewriting the operator definition of Green's function as $(E_t - \hat{H})\hat{G} = \hat{1}$ and projecting it to the orbital basis, we obtain the Dyson's equations[20]

$$\sum_i \tilde{G}_{ki}(E_t S_{il} - H_{il}) = \delta_{kl} \tag{4}$$

where the matrix $\tilde{\mathbf{G}} = \mathbf{S}^{-1}\mathbf{G}\mathbf{S}^{-1}$ is the transformed Green's function matrix, identical to **G** for orthogonal basis.

In effectively one-dimensional chainlike bridges, ET coupling can be characterized by using decays per site. These decays can be defined as[12,16]

$$\epsilon_j = \frac{G_{i\,j+1}}{G_{ij}} \qquad j > i \tag{5}$$

where G_{ij} is the Green's function matrix element between backbone orbitals of ith and jth sites. A similar definition using the Green's function $\tilde{G}$ is

$$\tilde{\epsilon}_j = \frac{\tilde{G}_{i\,j+1}}{\tilde{G}_{ij}} \qquad j > i \tag{6}$$

For sufficiently long periodic bridges, boundary effects are negligible, and these decays are identical for all orbitals far enough from the boundaries. Therefore, in the remainder of the paper, we will remove the subscripts for ϵ and $\tilde{\epsilon}$. Also, it can be shown that $\tilde{\epsilon}$ is identical to ϵ regardless of whether the basis is orthogonal or not.[28]

The decay per site can also be determined without computing the Green's function itself but by projecting the Schrödinger equation on the chosen basis and expanding the wave function using these basis orbitals. The resulting equations for the expansion coefficients are similar to the Dyson's equations (4):[11]

$$\sum_i C_i(E_t S_{il} - H_{il}) = 0 \tag{7}$$

For long enough bridges, the wave function decay can be assumed to be uniform;[12] i.e.,

$$C_{i+l\,\mathrm{m}} = \tilde{\epsilon}^m C_i \tag{8}$$

where l is the number of orbitals per site. $\tilde{\epsilon}$ can be found by solving the system of equations (7).

It is more convenient to characterize the decay per site by $\tilde{\epsilon} + 1/\tilde{\epsilon}$ rather than by $\tilde{\epsilon}$ for two reasons: $\tilde{\epsilon} + 1/\tilde{\epsilon}$ remains real inside the energy bands, where $\tilde{\epsilon}$ is complex, and it is technically easier to solve eqs 7 and 8 for $\tilde{\epsilon} + 1/\tilde{\epsilon}$.

Applications to Chainlike Bridges

Using our approach, we can now verify how several detailed features, that were not properly addressed by earlier simpler methods, affect the tunneling mechanism. For example, we now investigate the effects of next-to-NN interactions between orbitals, side groups, chain boundaries, and nonorthogonal

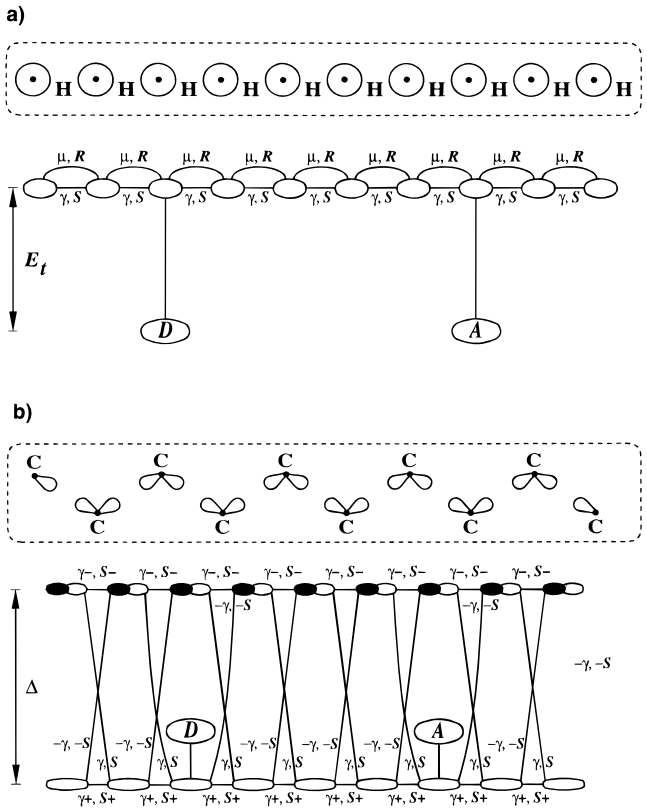

Figure 1. (a) Model chain 1, one orbital per site. γ and S are the NN coupling and overlap, and μ and R are the NNN coupling and overlap, respectively. E_t is the tunneling energy. (b) Model chain 2, two orbitals per site. γ_+ and S_+ are the NN coupling and overlap between two NN bonds, γ_- and S_- are between two antibonds, and γ and S are between a bond and an antibond. Δ is the energy gap between bonding and antibonding orbitals.

orbital basis. Analyses were performed for the following chainlike bridges:

(a) Model chain 1 is a periodic chain of ideal atoms with one orbital per site (Figure 1a, where γ, S and μ, R are the NN and NNN couplings and overlaps, respectively). The atoms have been parameterized as hydrogens. The distance between them has been chosen to make the ratio of NNN to NN couplings, μ/γ, close to the ratio for the next two chains.

(b) Model chain 2 is a periodic chain of atoms with two orbitals per site (Figure 1b shows only NN couplings γ and overlaps S for the bond/antibond basis set, but all terms up to NNN are retained in the calculations). The indices "+" and "−" refer to the bond−bond and antibond−antibond couplings and overlaps, respectively; bond−antibond couplings and overlaps are unindexed. This chain can be thought of as the backbone of an alkane chain, so the atoms are represented as simplified carbons.

(c) The alkane chain C_nH_{2n+2} has six orbitals per site (Figure 2, no couplings and overlaps are shown for clarity). Standard parameters have been used for carbon and hydrogen atoms.[24]

Results and Discussion

The numerical calculations have been performed for finite bridges, while the condition of uniform wave function decay (eq 8) employed in the analytical calculations is valid only for infinite chains. Therefore, the first issue that arises when comparing the numerical and analytical results is how significant are the chain boundary effects? This point has been examined in two ways: by analytically solving the exact Dyson's equations (4) for finite chain lengths and by numerical calculations. For example, the semiinfinite model chain 1 in the NN approximation has Green's function matrix elements[29]

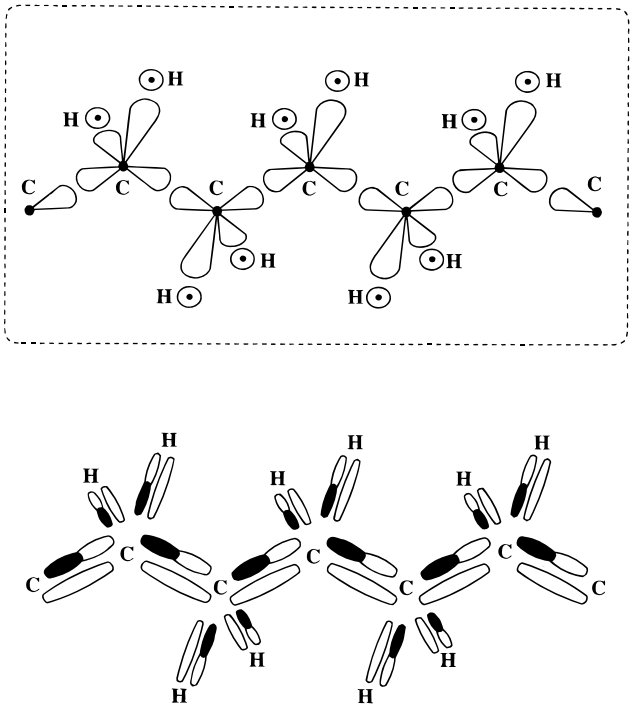

Figure 2. Alkane chain, six orbitals per site. For clarity, the donor and acceptor sites and the interactions between orbitals are not shown.

$$\tilde{G}_{kl} = \tilde{\epsilon}^{l-k}\tilde{G}_{kk} \qquad l \geq k \geq 1 \tag{9}$$

$$\tilde{G}_{kk} = \frac{1-\tilde{\epsilon}^{2k}}{1-\tilde{\epsilon}^{2}}\tilde{G}_{11} \tag{10}$$

$$\tilde{G}_{11} = -\frac{\tilde{\epsilon}}{E_t S - \gamma} \tag{11}$$

$$\tilde{\epsilon} + \frac{1}{\tilde{\epsilon}} = -\frac{E_t - \alpha}{E_t S - \gamma} \tag{12}$$

where α is the orbital energy and k and l are the orbitals connected to D and A, respectively. Notice that the decay per site $\tilde{\epsilon}$ is independent of the choice of connection sites k and l, and the Green's function matrix elements $\tilde{G}_{kl}$ converge rapidly to the infinite chain values as k increases ($|\tilde{\epsilon}| < 1$ for E_t outside the energy band). Similar behavior is obtained from the numerical calculations of model chain 2 (with and without NN approximation and for both zero and non-zero overlaps). The results for the Green's function matrix elements for various chain lengths (20, 50, and 100 sites) and with the location of D and A connection sites varying all over the chain, but at fixed separation (10 sites), have been computed. The matrix elements are the same within an accuracy better than 1% if the connection sites are further than five sites from the chain boundaries. Another issue is the breakdown of exponential distance decay for small separations between the connection sites. It has been found that the value of ϵ is almost invariant for separations larger than 10 sites. To avoid these problems, all the remaining numerical calculations have been performed for connection sites separated at least 10 sites from the chain boundaries and between

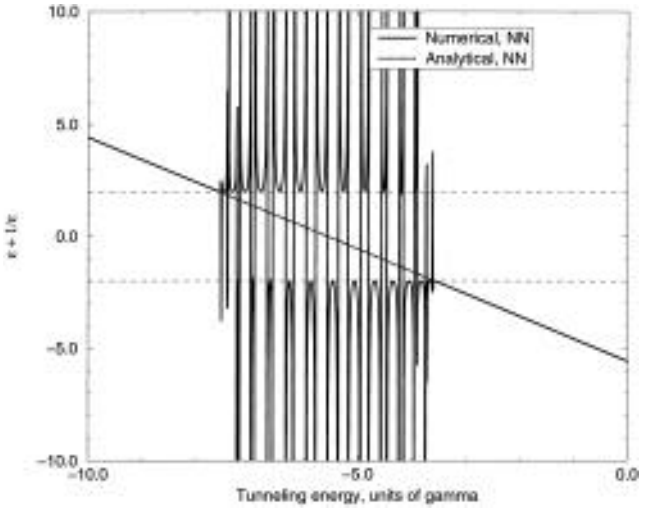

Figure 3. Comparison between the numerical and analytical results for model chain 1 (the zero overlap case). The chain is 50 sites long, and the donor and acceptor connection orbitals are located at sites 20 and 35. Thin dashed lines show $\epsilon + 1/\epsilon = \pm 2$.

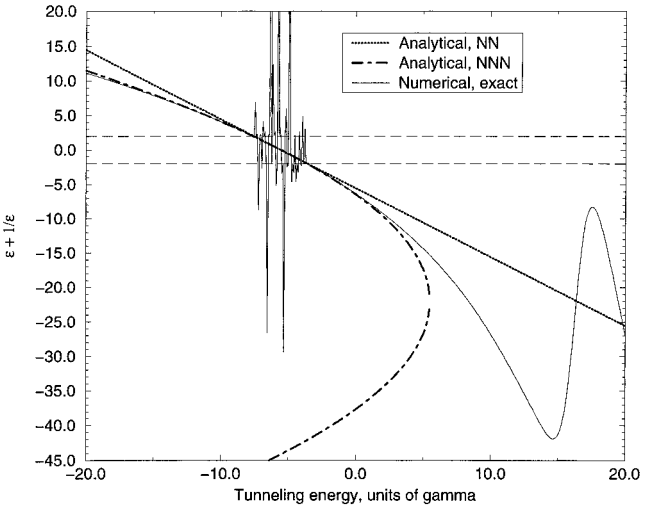

Figure 4. Green's function decay as a function of the tunneling energy for model chain 1 (zero overlap). The chain length and location of the donor and acceptor connection sites are described in Figure 3. In this and the following figures, the analytical solutions are shown only for the energies where they are real.

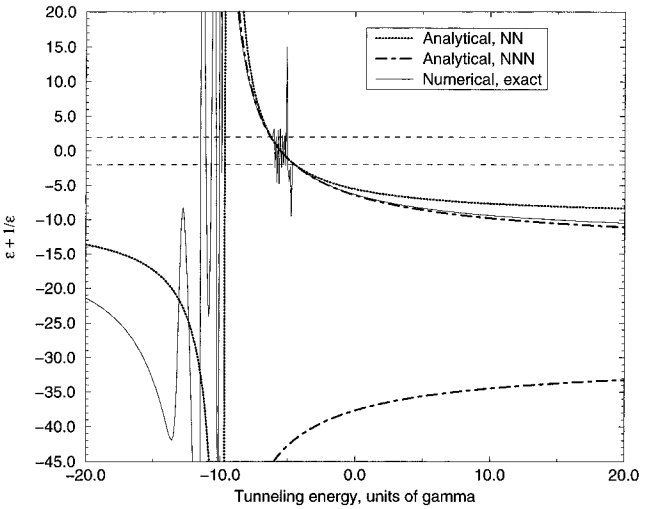

Figure 5. Green's function decay as a function of the tunneling energy for model chain 1 (non-zero overlap). The chain length and location of the donor and acceptor connection sites are described in Figure 3.

them. Similar results have been obtained for chainlike molecular wires (with the focus on STM imaging) using a scattering formalism.[30]

A comparison between the decays obtained analytically and the ones computed numerically for model chain 1 (with no overlap and in the NN approximation) is shown at Figure 3. The two results are identical outside the energy band. Inside the band, however, differences occur because of the different boundary conditions employed by the analytical and numerical methods (the results are extremely sensitive to boundary conditions, since the wave function is delocalized). In the first case, $\tilde{\epsilon}$ defined by eqs 7 and 8 is a mere phase factor $e^{i\phi(E_t)}$ inside the band ($-\pi < \phi(E_t) < \pi$ is a monotonic function within the band—infinite chain limit). Thus, $\tilde{\epsilon} + 1/\tilde{\epsilon} = 2 \cos \phi(E_t)$, and the relation $|\tilde{\epsilon} + 1/\tilde{\epsilon}| \leq 2$ is used for determining the energy band. In the numerical calculations, ϵ defined in eq 5 is real, and $|\epsilon + 1/\epsilon| \geq 2$ at any E_t (finite chain). Inside the energy band, the decay shows first-order polelike singularities:

$$\epsilon = \frac{\cos(d+1)\phi(E_t)}{\cos d\phi(E_t)} \tag{13}$$

where d is the D−A separation. These types of behavior of the analytical and numerical results inside the energy bands are generic. We will not discuss any further details, since we are primarily interested in ET occurring outside the energy bands.

We now consider the wave function decays for the model chain 1 shown at Figures 4 and 5 for zero and non-zero overlaps, respectively. First, we emphasize that the numerical dependence of $\epsilon + 1/\epsilon$ on E_t presents two main types of behavior: regular (slowly varying with E_t) and oscillatory. As mentioned above, the oscillatory dependence *inside* the band is related to the *poles* of the Green's function corresponding to the eigenstates. Oscillatory behavior *outside* the band, however, originates from interference between different orders of interaction. For physically relevant parameters, close to the band, the dependence is always regular.

Notice that, for any molecular structure, the numerical approach always gives a single solution for eq 3. The analytical results in the NN approximation (eq 12) are compared to the numerical ones in the energy range of regular behavior. As expected, both functions are close to each other near the energy band but deviate as $|E_t|$ increases. Adding the NNN interactions, however, changes the situation qualitatively: the analytical results have *two* different branches

$$\tilde{\epsilon}_{1,2} + \frac{1}{\tilde{\epsilon}_{1,2}} = -\{(E_tS - \gamma) \mp [(E_tS - \gamma)^2 - 4(E_tR - \mu)((E_t - \alpha) - 2(E_tR - \mu))]^{1/2}\}/[2(E_tR - \mu)] \tag{14}$$

They describe two possible decay regimes for the wave function along the same physical pathway, each of them with a different dependence of $\tilde{\epsilon}$ on E_t.[31] The solutions are associated with two ET *decay modes* along the pathway. Roughly, the electron can propagate via transitions either between NN orbitals coupled by γ or between NNN orbitals coupled by μ. Each mode of electron propagation is a mixture of both transitions characterized by a specific decay per site.

Relative contributions of the NN and NNN transitions to each ET mode can be examined by a perturbative approach, since the NNN couplings and overlaps are much smaller than the NN ones. Depending on the tunneling energy, the solutions are

either both real (notice that at those energies, the numerical results are regular) or complex conjugated (the numerical results oscillate). In the first regime, one of the NNN solutions is close to the NN result, while in the other one, both solutions differ substantially from the NN result and the numerical calculations. Here, we can define a small parameter δ as

$$\delta \approx |\frac{\mu}{\gamma}| \approx |\frac{R}{S}| \ll 1 \tag{15}$$

Expanding eq 14 over δ gives, for physically relevant energies,[32]

$$\tilde{\epsilon}_1 + \frac{1}{\tilde{\epsilon}_1} = -\frac{E-\alpha}{ES-\gamma} + O(\delta)$$
$$\tilde{\epsilon}_2 + \frac{1}{\tilde{\epsilon}_2} = -\frac{ES-\gamma}{ER-\mu} + O(1) \tag{16}$$

Comparing solution 1 with eq 12 indicates that NN transitions dominate this mode, while NNN transitions provide small corrections. None of the transitions dominate the second mode. This mode is much more localized ($|\tilde{\epsilon}_2| \ll |\tilde{\epsilon}_1|$ for the entire range of tunneling energies).[33] Obviously, at energies where the solutions are complex conjugated, none of the NNN solutions are close to either the NN solution or the numerical calculations, and none of the transitions dominate either of the ET modes.

In general, we can take into account not only NN and NNN but also higher orders of interactions up to order n. In this case, we will have n decay modes, one with the NN transitions dominating and higher order transitions contributing as minor corrections for the energies near the band. Since eqs 7 and 8 are linear, the Green's function matrix element can be represented as a superposition of all ET decay modes:

$$G_{ij} \sim \sum_{\lambda} \tilde{C}_{\lambda} \tilde{\epsilon}_{\lambda}^{j-i} \tag{17}$$

where λ is the mode index and the intensities $\tilde{C}_{\lambda}$ are determined by the overlap mixing of the D and A orbitals with the bridge ET modes. In the energy range where only one of the modes has the largest decay in absolute value $\tilde{\epsilon}_0$, we can write the total decay ϵ as

$$\epsilon = \frac{\sum_{\lambda} \tilde{C}_{\lambda} \left(\frac{\tilde{\epsilon}_{\lambda}}{\tilde{\epsilon}_0}\right)^{j-i+1}}{\sum_{\lambda} \tilde{C}_{\lambda} \left(\frac{\tilde{\epsilon}_{\lambda}}{\tilde{\epsilon}_0}\right)^{j-i}} \epsilon_0 \tag{18}$$

For large D−A separations, i.e., when $j - i \gg 1$, all the terms, except the contribution from the mode 0, vanish in both sums, and the total decay per site is approximately ϵ_0. In other words, only one, the least localized, mode "survives" at long enough distances. In the case where ϵ is dominated by two modes with complex conjugated decays (the ones with the largest real part in the absolute value), the Green's function not only decays but also oscillates along the chain.

The concept of ET decay modes is very important since it provides us with a simple view of the ET mechanisms along a physical pathway as a superposition of several modes. It gives a simple method to decompose an apparently complicated dependence of the Green's function matrix element G_{DA} on the tunneling energy E_t into several distinct contributions.

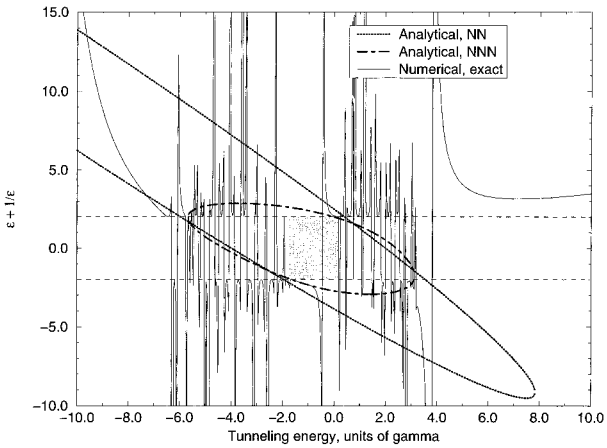

Figure 6. Green's function decay as a function of the tunneling energy for model chain 2 (zero overlap). The chain length and location of the donor and acceptor connection sites are described in Figure 3. Physically relevant tunneling energies fall in the energy gap (marked with the gray box).

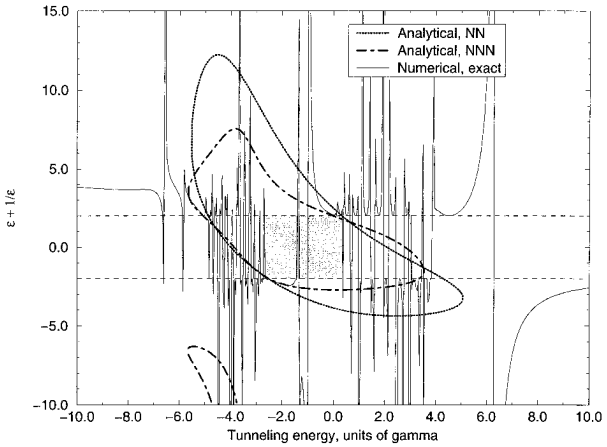

Figure 7. Green's function decay as a function of the tunneling energy for model chain 2 (non-zero overlap). The chain length and location of the donor and acceptor connection sites are described in Figure 3. In this and the following figures, physically relevant tunneling energies fall in the energy gap (marked with the gray box).

The effects of a nonorthogonal basis can be analyzed by comparing Figures 4 and 5. The decay per site is much less sensitive to the tunneling energy in the case of non-zero overlaps. This is, in fact, a generic feature due to partial compensation of interaction and overlap terms in eqs 3, 4, and 7. It also explains, in part, why the *Pathway* model, assuming E_t-independent decays, provides qualitatively correct results.

Model chain 2 can be discussed in terms of either a bond or a hybrid orbital basis set. This distinction is essential, because the same order of interactions between orbitals corresponds to different physical interactions in a bond and a hybrid basis. Even the simplest NN approximation in a bond basis includes the NN, NNN, and next-to-NNN interactions between hybrid orbitals. The NN and NNN approximations in a hybrid basis, however, omit some terms of comparable size, making the approach inconsistent. Therefore, a bond orbital basis set is more appropriate for these ET calculations.

The results for model chain 2 are shown at Figures 6 and 7 for zero and non-zero overlaps, respectively. The unit cell for this chain consists of two orbitals, generating two energy bands (valence and conduction bands). There are two analytical solutions in the NN approximation. Close to the bands, both solutions are real, while further from the bands, they are complex conjugated. There are two transitions between real and complex

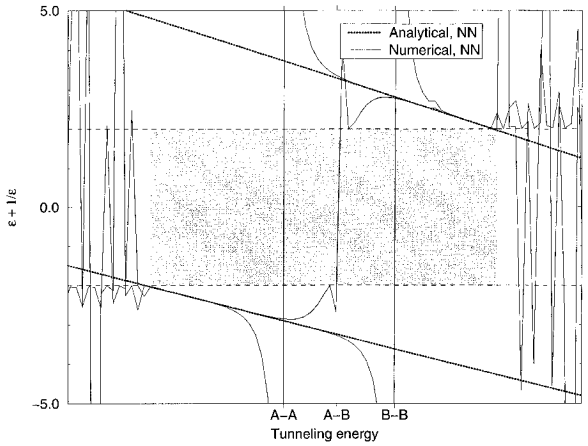

Figure 8. Transition energies for different symmetries of the connecting orbitals for model chain 2 (zero overlap and NN approximation). The chain length and location of the donor and acceptor connection sites are described in Figure 3. The transition energies in increasing value correspond to donor and acceptor connected via two antibonding orbitals, a bonding orbital and an antibonding orbital (the transition energy is E_0), and two bonding orbitals, respectively.

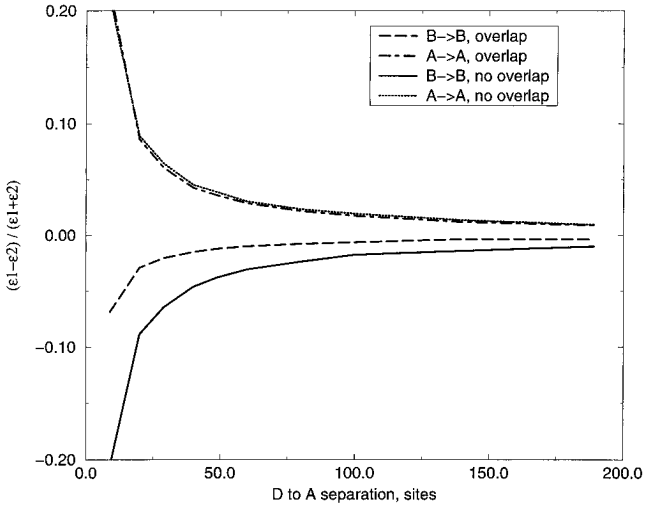

Figure 9. Relative difference of the decays at the two extreme transition energies (both donor and acceptor connected to two bonding orbitals and two antibonding orbitals, respectively) as a function of the donor−acceptor separation for model chain 2 (NN approximation). The chain length is 220 sites; D is connected to site 21.

conjugated solutions, where G_{DA} changes from regular to oscillatory. At these transitions, both real and imaginary parts of the solutions show bifurcation-like behavior.

In the energy gap, different modes have opposite signs for the decay per bond; therefore, they compete with each other (destructive interference). One of them dominates at the energies near the valence band, while the other one dominates near the conduction band. As the tunneling energy increases, a transition from one dominating mode to the other one occurs in the middle of the gap. At the transition energy, G_{DA} is zero, since the contributions from both modes annihilate each other. The transition energy is close to where both decays are the same in absolute value (E_0) but also depends on the bonding or antibonding symmetry of the connecting orbitals, as shown at Figure 8 (for the zero overlap case). This can be understood from eq 18, which shows that the dominating mode is determined by two factors: the decay per bond $\tilde{\epsilon}_\lambda$ and the mode intensity $\tilde{C}_\lambda$. The first and most important one depends exclusively on the mode, while the second one is also dependent on the symmetry of the connecting orbitals.[34] The ET mode dominating near the HOMO (which includes mostly bonding orbitals) has a stronger coupling with bonding connecting orbitals, while the other mode (which includes mostly antibonds) has a stronger coupling with antibonding ones. Therefore, for G_{ij}'s that have both connecting orbitals bondlike, the mode dominating near the HOMO is more intensive, and the transition energy is higher than E_0. If both connecting orbitals are antibond-like, the mode dominating near the LUMO is more intensive, and the transition energy is lower than E_0. In the case when one connecting orbital is bondlike and the other one is antibond-like, both ET modes have the same intensity, and the transition energy is exactly E_0.

Equation 18 shows that, as the D−A separation increases, ϵ becomes more and more controlled by the dominating mode, and the transition energies converge to E_0. This is illustrated at Figure 9, where the relative difference of the two decays at the transition energies for different symmetries of the connecting orbitals as a function of the D−A separation is shown. However, for physically relevant D−A separations, even as long as several dozen sites, the difference in the transition energies remains noticeable.

As for model chain 1, inclusion of NNN interactions between the orbitals doubles the number of modes. Two of the NNN

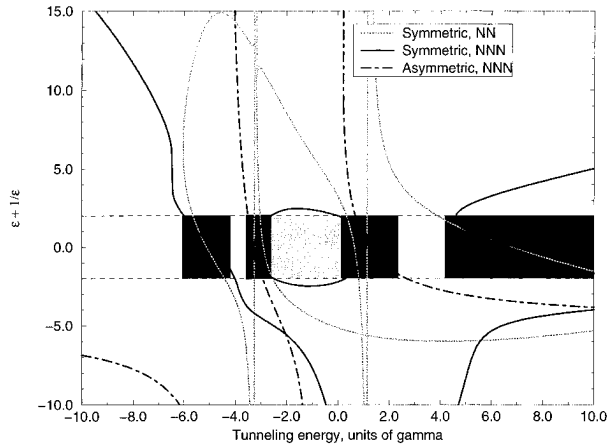

Figure 10. Green's function decay as a function of the tunneling energy for an alkane bridge (non-zero overlap). The chain length and location of the donor and acceptor connection sites are described in Figure 3. For clarity, only analytical results are shown, and the energy bands (computed numerically) are marked with the darker gray boxes.

modes are close to the NN ones in the energy range that their decays are real (and the numerical results are regular). The agreement is better for non-zero overlap due to the partial compensation of interaction and overlap terms. Also, these NNN solutions are in good agreement with the numerical results (except around E_0). The other two NNN modes are never close to either the NN modes or the numerical results.

The numerical results show three apparent transitions for non-zero overlaps (Figure 7). They appear because of interference of higher order interactions between orbitals. One of the Green's function matrix elements in eq 5 crosses zero twice, something that does not happen in either the NN or the NNN approximations (higher order interactions slightly broaden the transition range).

The results for the alkane chain are shown at Figure 10 (only non-zero overlaps, for briefness). For clarity, only the analytical solutions are shown, and the energy bands computed numerically are marked with gray boxes. The analytical calculations have been performed using a bonding/antibonding orbital basis set, with the caveat that the C−H orbitals have been transformed into their symmetric and antisymmetric combinations. In the transformed basis, eqs 7 and 8 describe two independent

subsystems: one includes the backbone and the symmetric combinations of C−H orbitals and the other consists of the antisymmetric combinations of C−H orbitals. The subsystems do not interact with each other, and the ET decay modes are analyzed separately. In the NN approximation, antisymmetric orbitals do not interact at all. Four symmetric modes determining four energy bands are roughly similar to the solutions for model chain 2 in the NN approximation. Also, the analytical results are in qualitative agreement with the numerical calculations within the main energy gap but strongly deviate at other energies.

In the NNN approximation, there are two antisymmetric and six symmetric ET modes. Up to four symmetric modes have real decays per bond. They are similar to the NN modes only within the two extreme energy bands (that are determined by symmetric modes). The other two, valence and conduction, bands consist of overlapping contributions from both symmetric and antisymmetric modes. The HOMO's and LUMO's are symmetric states, but the bottom of the valence band and the top of the conduction band are determined by the antisymmetric modes. In the energy gaps between the extreme bottom and the valence bands, as well as between the conduction and the extreme top bands, two modes with complex conjugated decays dominate.

Most important, however, is the mode behavior in the main energy gap between the HOMO and LUMO, where realistic D and A states exist. It is qualitatively similar to the results for model chain 2, although the structure of the ET decay modes for the alkane chain is much more complex. Again, in this gap, two major modes have real decays with opposite signs, and they compete with each other. One mode dominates near the valence band and the other one dominates near the conduction band. There is a narrow transition range in the middle of the gap, where the Green's function matrix element goes through zero. Another interesting feature is the weak dependence of the decays on the tunneling energy within the gap (except around E_0).

Similarly to the other chains, the NNN results for alkanes are in very good agreement with the numerical calculations at the tunneling energies where a single mode dominates (the numerical results show regular behavior). Since the tunneling energies typical for ET in chemical systems and biological molecules fall in this range, these results indicate that including only the NN and NNN interactions between orbitals is sufficient for quantitative calculations with pathwaylike models.

Conclusions

We have studied the conditions for validity of simple pathwaylike models based on exact and approximate extended Hückel level Hamiltonians. An important conclusion is that these models are able to provide a quantitative description of ET when only the nearest and next to nearest neighbor interactions between orbitals are included in the Hamiltonian.[35] The effects of higher order interactions are negligible. The NNN interactions are vital for quantitative calculations. To obtain the correct E_t dependence of the decay per site, consistent with the very weak experimental dependence, nonorthogonality of the orbital basis has to be included.

Electron transfer along a single physical pathway can be naturally understood in terms of the ET decay modes. It provides a simple view of the entire ET electronic coupling along the pathway as a result of the competition among these modes, making an apparently complicated dependence of the Green's function matrix element G_{DA} on the tunneling energy E_t clear. Most importantly, in the main energy gap (the range of physically relevant tunneling energies), ET is determined by the competition between only two major modes, even though the bridge may have a complex orbital structure. These modes have real decays but opposite signs, with one of them dominating near the valence band and the other one near the conduction band. In the middle of the gap, close to the energy where both decays have the same absolute value, a transition between them occurs. At this point, the Green's function crosses zero because of destructive interference between the two major modes. Also, it is important that tunneling energies typical for biological ET (up to 4−5 eV above HOMO) fall in the range below the transition. In that range, only one ET mode dominates, and the decay per site is always negative. As such, the sign of the wave function alternates every bond, as the *Pathway* model assumes.

The pathway approach and the concept of ET decay modes should be considered complementary. The second one provides a comprehensive description of ET along a single physical tube of pathways, while the first one explains structural effects (interference among different pathways and nonlocal interactions). In general, both concepts are needed for an adequate description of ET in molecules with nontrivial geometric and electronic structure. This paper provides a framework to develop new effective (E_t-dependent) interaction parameters for pathwaylike Hamiltonians that will be used for quantitative predictions of ET in chemical and biological molecules.

Acknowledgment. We thank Nick Socci and David Beratan for helpful discussions. This research has been supported by NIH (Grant GM48043).

References and Notes

(1) Marcus, R. A.; Sutin, N. *Biochim. Biophys. Acta* **1992**, *811*, 265.
(2) McConnell, H. M. *J. Chem. Phys.* **1961**, *35*, 508.
(3) Langen, R.; Chang, I.-J.; Germanas, J. P.; Richards, J. H.; Winkler, J. R.; Gray, H. B. *Science* **1995**, *268*, 1733.
(4) Newton, M. D. *Chem. Rev.* **1991**, *91*, 767.
(5) Ratner, M. A. *J. Phys. Chem.* **1990**, *94*, 4877.
(6) Curtiss, L. A.; Naleway, C. A.; Miller J. R. *Chem. Phys.* **1993**, *176*, 387.
(7) Kuki, A.; Wolynes, P. G. *Science* **1987**, *236*, 1647.
(8) Stuchebrukhov, A. A.; Marcus, R. A. *J. Chem. Phys.* **1995**, *99*, 7581.
(9) Regan, J. J.; Risser, S. M.; Beratan, D. N.; Onuchic, J. N. *J. Phys. Chem.* **1993**, *97*, 13083.
(10) Beratan, D. N.; Onuchic, J. N.; Hopfield, J. J. *J. Chem. Phys.* **1987**, *86*, 4488.
(11) Onuchic, J. N.; Beratan, D. N. *J. Chem.Phys.* **1990**, *92*, 722.
(12) Beratan, D. N.; Hopfield, J. J. *J. Am. Chem. Soc.* **1984**, *106*, 1584.
(13) Beratan, D. N.; Onuchic, J. N.; Winkler, J. R.; Gray, H. B. *Science* **1992**, *258*, 1740.
(14) The general expression for nonorthogonal basis has been recently obtained. See: Priyadarshy, S.; Skourtis, S.; Risser, S. M.; Beratan, D. N. *J. Chem. Phys.*, in press.
(15) Evenson, J. W.; Karplus, M. *J. Chem. Phys.* **1992**, *96*, 5272.
(16) Onuchic, J. N.; de Andrade, P. C. P.; Beratan, D. N. *J. Chem. Phys.* **1991**, *95*, 1131.
(17) Gruschus, J. M.; Kuki, A. *J. Phys. Chem.* **1993**, *97*, 5581.
(18) Siddarth, P.; Marcus, R. A. *Phys. Chem.* **1993**, *97*, 2400.
(19) Broo, A.; Larsson, S. *Chem. Phys.* **1992**, *161*, 363.
(20) Shephard, M. J.; Paddon-Row, M. N.; Jordan, K. D. *J. Am. Chem. Soc.* **1994**, *116*, 5328.
(21) Da Gama, A. A. S. *J. Theor. Biol.* **1990**, *142*, 251.
(22) Beratan, D. N.; Betts, J. N.; Onuchic, J. N. *Science* **1991**, *252*, 1285.
(23) Regan, J. J.; Di Bilio, A. J.; Langen, R.; Skov, L. K.; Winkler, J. R.; Gray, H. B.; Onuchic, J. N. *Chem. Biol.* **1995**, *2*, 489.
(24) Curry, W. B.; Grabe, M. D.; Kurnikov, I. V.; Skourtis, S. S.; Beratan, D. N.; Regan, J. J.; Aquino, A. J.; Beroza, P. P.; Onuchic, J. N. *J. Bioenerg. Biomembr.* **1995**, *27*, 285.
(25) Yates, H. *Huckel Molecular Orbital Theory*; Academic: New York, 1978.
(26) Development of new sets of Hückel parameters more appropriate for ET calculations is now being attempted. Kurnikov, I.; Beratan, D. Personal communication.

(27) Naray-Szabo, G. *Applied quantum chemistry*, Dordrecht: Boston, 1987.

(28) For periodic molecules, the overlap matrix elements are $S_{ij} = s_{|i-j|}$ and $s_0 = 1$, and from eq 6, the relationship between the regular and transformed Green's functions is $G_{ij} = \tilde{G}_{ij}[1 + (\tilde{\epsilon} + 1/\tilde{\epsilon})s_1 + (\tilde{\epsilon}^2 + 1/\tilde{\epsilon}^2)s_2 + ...]^2$. Therefore, the ratio given by eq 5 makes $\epsilon = \tilde{\epsilon}$.

(29) Equations 9−12 are obtained by explicitly solving the Dyson's equations (4) with the Hamiltonian $H_{ij} = \alpha\delta_{ij} + \gamma\delta_{|i-j|,1}$ and overlap matrix $S_{ij} = \delta_{ij} + S\delta_{|i-j|,1}$, where $i, j > 0$.

(30) Mujica, V.; Kemp, M.; Ratner, M. A. *J. Chem. Phys.* **1994**, *101*, 6849, 6855.

(31) The relations between $\tilde{\epsilon}$ and E_t, given by eq 16, are, basically, **dispersion relations** ($\tilde{\epsilon}$ can be considered to be a complex wave vector). Therefore, their branches are associated with **modes**.

(32) The expansion given by eq 16 breaks down for large tunneling energies (for example, $E_t \sim \pm|\gamma^2/\mu|$, for zero overlap). Inclusion of overlap extends the range of validity of the expansion. In any case, the breakdown occurs at energies that are not physically relevant.

(33) For physically relevant tunneling energies (close enough to the band), the solutions are real. Since we are primarily interested in ET at these energies, the analytical solutions are shown at Figures 3−8 and 10 only for the energies that they are real.

(34) Connecting orbitals are the bridge orbitals directly coupled to D and A. They are represented by the indices *i* and *j* in eq 2. As expected, the intensity of these couplings will depend on the symmetry of D and A.

(35) For the chainlike bridges studied above, the NN and NNN interactions are dominant. This may not be true for bridges with more complex structures. Thus, certain higher order interactions (such as, e.g., "cross-talks"[12]) may have to be included into the Hamiltonian.

JP953568G